Adhesion and Nanomechanics of Pili from the Probiotic *Lactobacillus rhamnosus* GG

Prachi Tripathi,[†,‡,∥] Audrey Beaussart,[†,∥] David Alsteens,[†] Vincent Dupres,[†] Ingmar Claes,[‡,§] Ingemar von Ossowski,[⊥] Willem M. de Vos,[⊥] Airi Palva,[⊥] Sarah Lebeer,[‡,§] Jos Vanderleyden,[‡,*] and Yves F. Dufrêne[†,*]

[†]Institute of Life Sciences, Université catholique de Louvain, Croix du Sud, 1, bte L7.04.01, B-1348 Louvain-la-Neuve, Belgium, [‡]Centre of Microbial and Plant Genetics, KU Leuven, Kasteelpark Arenberg 20, box 2460, B-3001 Leuven, Belgium, [§]Department of Bioscience Engineering, Universiteit Antwerpen, Groenenborgerlaan 171, B-2020 Antwerpen, Belgium, and [⊥]Department of Veterinary Biosciences, University of Helsinki, Helsinki, Finland, P.O. Box 66, FIN-00014 Helsinki, Finland. [∥]These authors contributed equally to this work.

ABSTRACT Knowledge of the mechanisms by which bacterial pili adhere to host cells and withstand external forces is critical to our understanding of their functional roles and offers exciting avenues in biomedicine for controlling the adhesion of bacterial pathogens and probiotics. While much progress has been made in the nanoscale characterization of pili from Gram-negative bacteria, the adhesive and mechanical properties of Gram-positive bacterial pili remain largely unknown. Here, we use single-molecule atomic force microscopy to unravel the binding mechanism of pili from the probiotic Gram-positive bacterium *Lactobacillus rhamnosus* GG (LGG). First, we show that SpaC, the key adhesion protein of the LGG pilus, is a multifunctional adhesin with broad specificity. SpaC forms homophilic trans-interactions engaged in bacterial aggregation and specifically binds mucin and collagen, two major extracellular components of host epithelial layers. Homophilic and heterophilic interactions display similar binding strengths and dissociation rates. Next, pulling experiments on living bacteria demonstrate that LGG pili exhibit two unique mechanical responses, that is, zipper-like adhesion involving multiple SpaC molecules distributed along the pilus length and nanospring properties enabling pili to resist high force. These mechanical properties may represent a generic mechanism among Gram-positive bacterial pili for strengthening adhesion and withstanding shear stresses in the natural environment. The single-molecule experiments presented here may help us to design molecules capable of promoting or inhibiting bacterial—host interactions.

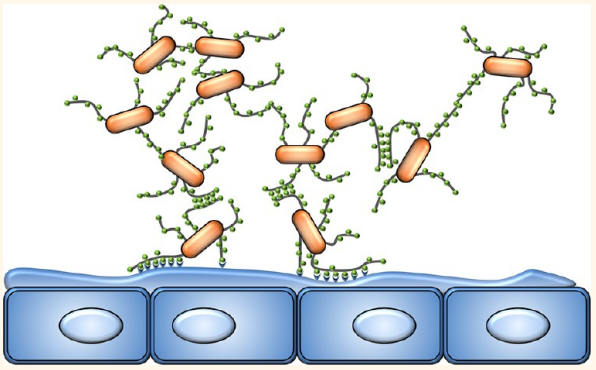

KEYWORDS: bacterial pili · adhesion · nanomechanics · probiotics · AFM · force spectroscopy · single-molecule manipulation

Probiotic bacteria are thought to contribute to human health through several mechanisms, including competitive exclusion of pathogenic bacteria, reinforcement of the intestinal epithelial barrier, and modulation of the immune system of the host, particularly in the small intestine.[1−7] Consequently, probiotics have great potential in the prevention and treatment of gastrointestinal infections, inflammatory conditions, and allergic reactions or as carrier and adjuvant in vaccination.[8,9] Bacterial cell surface constituents play key roles in establishing tight interactions between probiotics and their host.[10−12] In the Gram-positive species *Lactobacillus rhamnosus* GG (LGG), key players in promoting adhesive interactions with mucus and epithelial cells are the recently discovered cell surface pili.[13,14] LGG cells contain multiple pili, averaging 10 to 50 per cell, and with lengths of up to 1 μm.[13] Comparative genomics has revealed the presence of a gene cluster which encodes SpaCBA polymeric pili exhibiting an intestinal mucus-binding capacity and which is not present in less adherent related strains such as *L. rhamnosus* Lc705.[13] While the adhesive and mechanical properties of pili from Gram-negative bacteria have been widely investigated using various single-molecule techniques,[15−22] the biophysical properties of pili from LGG and other Gram-positive bacteria remain largely unknown.

* Address correspondence to jozef.vanderleyden@biw.kuleuven.be, yves.dufrene@uclouvain.be.

Received for review February 11, 2013 and accepted March 16, 2013.

Published online March 26, 2013
10.1021/nn400705u

LGG pili are composed of three pilin subunits. SpaA is the major fiber component building up the pilus shaft, while SpaB and SpaC are the minor fiber components.[13] Mass spectrometry analysis has revealed a SpaA/SpaC/SpaB ratio of 5:2:1. SpaC has a central role in adhesion as it is responsible for binding to human mucus and intestinal epithelial cells.[13,14] This subunit is localized at the pilus tip, but also along the length of the pilus shaft, enabling bacteria to establish both long distance and intimate contact with host tissues.[23] The SpaC pilin subunit is an 895 residue protein (Figure 1a, top) whose primary structure analysis predicts the presence of a stretch of residues similar to the type A domain of von Willebrand factor (137−262) and three domains also present in the collagen-binding protein of *Staphylococcus aureus*: a repeat unit of collagen-binding protein domain B (cd00222) (residues 496−551) and two Cna protein B-type domains (pfam05738) (621−681 and 749−818).[13] These domains do not mediate binding in the collagen-binding protein of *S. aureus* but rather function as a stalk that presents the ligand-binding domain away from the bacterial surface.[24] The three-dimensional structure of SpaC is not available yet, but some general structural features may be inferred from the known structure of related pilins. Starting in 2007, structural analyses of major and minor pilins from Gram-positive bacteria have revealed a common modular structure of tandem immunoglobulin (Ig)-like domains joined end-on-end and stabilized by intramolecular isopeptide bonds.[25] Ig-like domains consist of multiple β-strands decorated with inserted helices, strands, and loops. In the important Gram-positive model *Corynebacterium diphtheriae*, the shaft SpaA pilin is a three Ig-like domain protein with a single CnaA-type domain inserted between two CnaB domains.[26] A unique feature of Gram-positive bacterial pili is the presence of internal isopeptide bonds not known in other proteins and formed autocatalytically between the side chains of Lys and Asn residues. These covalent cross-links are believed to help pili resist shear stresses while being engaged in host−cell interactions.[27]

Unlike the other pilins, minor pilins found at the pilus tip, like SpaC, possess additional domains with specialized adhesive functions.[25] The two available structures for such minor pilins (RrgA from *Streptococcus pneumoniae* and Cpa from *S. pyogenes*) have revealed the presence of adhesion domains that bind collagen and show features that are characteristic of eukaryotic adhesion proteins.[28,29] For instance, RrgA from *S. pneumoniae* is an elongated molecule, approximately 20 nm long, and composed of four independent domains.[29] The four domains are associated through flexible regions, such as short linkers and hairpins, suggesting that the full-length protein, once associated to the RrgB backbone fiber, could display a considerable level of domain flexibility. This modular and flexible organization could be important for the recognition of different host targets during infection, while the presence of two isopeptide bonds in the Ig domains would guarantee stability of the individual domains.[29]

In the past years, atomic force microscopy (AFM) has provided new insights into the specific binding forces of a variety of microbial species, including *Escherichia coli*,[17] *Mycobacterium tuberculosis*,[30−32] *S. aureus*,[33,34] *Streptococcus mutans*,[35,36] and *Candida albicans*.[37−40] Here, we use single-molecule AFM to explore the adhesion and mechanics of the LGG pilus. The results show that SpaC pilins bind with broad specificity and fast dissociation rate, and that the LGG pilus functions as a molecular zipper at low force and as a nanospring at high force. Consistent with the structural properties of Gram-positive pili, these biophysical properties may provide a powerful mechanism to piliated Gram-positives for strengthening adhesion and withstanding shear stresses.

RESULTS AND DISCUSSION

SpaC Mediates Homophilic Adhesion. To address single SpaC interactions, purified monomers were covalently attached on AFM tips with a ∼6 nm long PEG-benzaldehyde linker and on gold substrates modified with 10% COOH groups using NHS/EDC (Figure 1a, bottom). AFM imaging in aqueous solution confirmed the presence of a homogeneous, ∼2 nm thick SpaC monolayer on the substrate (Figure 1b).

As several microbial adhesins are known to mediate cell−cell aggregation through homophilic recognition,[31,37,39] we first asked whether SpaC is capable of forming such specific bonds. Figure 1c,d shows the adhesion force histogram with representative force−distance curves and the rupture length histogram recorded at a retraction speed of 1000 nm/s between a SpaC tip and a SpaC substrate. A substantial proportion of force curves (19%) showed single adhesion events with a mean adhesion force of 62 ± 17 pN (mean ± SD; total number of force curves = 600 from three different tips and substrates) and a rupture length ranging mostly from 30 to 110 nm. As can be seen in Figure 1e, a major reduction of adhesion frequency was observed upon addition of free anti-SpaC antibodies (top) or when performing the experiment with a tip functionalized with an irrelevant protein (BSA, bottom). These results demonstrate the specificity of our force measurements, thus indicating that the ∼62 pN force originates from SpaC−SpaC homophilic recognition.

Adhesion force peaks were well-described by the worm-like-chain (WLC) model,[41−43] using a persistence length of 0.4 nm: $F(x) = k_BT/l_p[0.25(1 - x/L_c)^{-2} + x/L_c - 0.25]$, where L_c and l_p are the contour length and persistence length of the molecule, k_B is the Boltzmann constant, and T the absolute temperature. The mean rupture force (∼60 pN) is larger than the unfolding

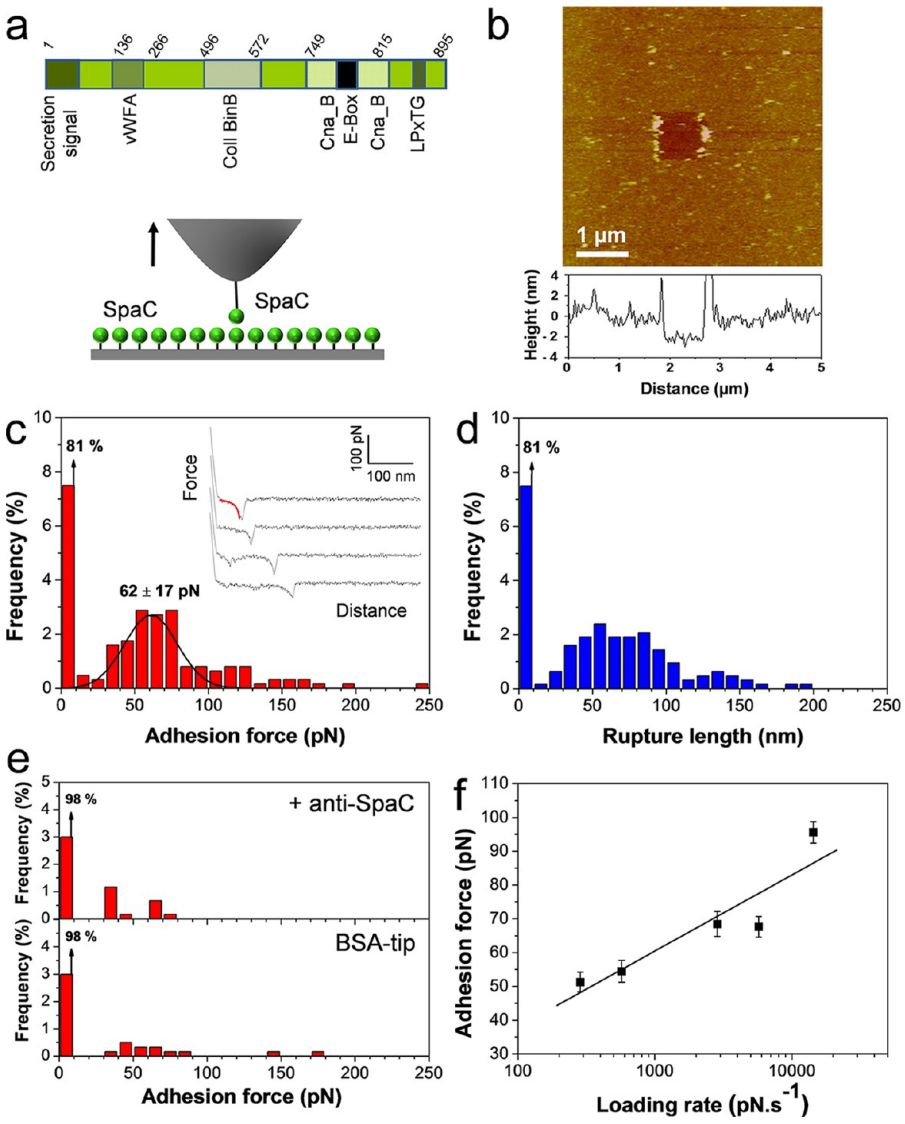

Figure 1. Force spectroscopy of the SpaC−SpaC interaction. (a) Primary structure of SpaC pilin subunit (see text for details). To measure SpaC−SpaC binding forces, SpaC monomers were attached randomly on a gold substrate and probed using a SpaC-tip. (b) AFM deflection image of a SpaC-coated substrate, together with a vertical cross section taken in the corresponding height image, recorded in buffer with a silicon nitride tip. A small area was first imaged at large forces (>10 nN) for short periods of time, followed by imaging a larger portion of the same area under normal load. Imaging at high forces resulted in pushing the grafted material aside, thereby confirming the presence of a 2.0 ± 0.5 nm thick protein monolayer on the surface. (c,d) Adhesion force histogram together with representative force curves (c) and rupture length histogram (d) obtained by recording force curves in buffer between a SpaC tip and a SpaC substrate. All curves were obtained using a contact time of 100 ms, a maximum applied force of 250 pN, and approach and retraction speeds of 1000 nm/s. The black line is a Gaussian fit to the data. Force peaks were well-described by the worm-like-chain model (red line on top curve in c). The data shown correspond to 600 force curves obtained from three independent experiments (different tips and substrates). (e) Control experiments showing a dramatic reduction of adhesion frequency when force measurements were performed in the presence of free anti-SpaC antibodies (top, *n* = 600) or with a BSA-coated tip (bottom, *n* = 600). (f) Plot of the SpaC−SpaC adhesion force as a function of the logarithm of the loading rate applied during retraction, while keeping constant the approach speed (1000 nm/s). Each data point in this plot represents the mean ± SEM (*n* = 200 force curves). A similar plot was obtained in a duplicate experiment using a different tip and substrate.

forces reported for α-helical domains (25−35 pN)[43] but clearly smaller than the forces needed to unfold β-folds domains, such as Ig domains (150−300 pN).[41] This indicates that SpaC Ig-like domains were not unfolded, which is also supported by our measured rupture lengths. Indeed, assuming that each amino acid residue contributes 0.36 nm to the contour length of a fully extended polypeptide chain and that SpaC is an 860 residue protein (without signal peptide), we expect that the length of a fully extended pilin should be *ca.* 300 nm. This value, added to the length of the PEG spacer (~6 nm), is much longer than the measured rupture lengths.

Accordingly, force profiles obtained for homophilic interactions reveal that Ig-like domains of SpaC pilins cannot be unfolded, a finding consistent with structural data showing that Gram-positive bacterial pilins are

mechanically stabilized by internal isopeptide bonds and with earlier AFM measurements revealing that Spy0128 pilins from the Gram-positive bacterium *S. pyogenes* are completely inextensible.[44] We suggest that the characteristic elongations of 30−110 nm may correspond, to some extent, to the straightening of the multiple modules and flexible regions of two SpaC pilins engaged in trans-interactions. This behavior would be consistent with the putative three-dimensional structure of SpaC, that is, an elongated protein made of multiple domains linked end-to-end through flexible regions like linkers and hairpins. As the measured SpaC−SpaC interactions are an average of forces between randomly immobilized proteins, it would be interesting in future research to investigate the interactions between oriented pilins.

Figure 1f shows that the SpaC−SpaC adhesion force (F) increased linearly with the logarithm of the loading rate (r), as observed for other receptor−ligand systems,[45−47] including homophilic interactions between mycobacterial adhesins[31] and between cadherins.[48] The length scale of the energy barrier, x_β, was assessed from the slope f_β ($1 \pm 0.2 \times 10^{-11}$) of the F *versus* ln(r) plot and found to be 0.4 nm, that is, in the range of values (0.2−1 nm) typically measured by single-molecule AFM.[45] Extrapolation to zero forces yielded $r_{F=0}$ ($2.7 \pm 0.5 \times 10^{-10}$) and, in turn, the kinetic off-rate constant of dissociation at zero force, $k_{off} = r_{F=0}x_\beta/k_BT = 0.2\ s^{-1}$. Such an off-rate, already reported for other adhesion proteins, such as cadherins[48] or influenza virus spike proteins,[49] means that individual pilins dissociate rapidly, thus that homophilic interactions are highly dynamic. This behavior is in contrast with the slow dissociation ($\sim 10^{-4}\ s^{-1}$) measured between the Gram-negative bacterial adhesive PapG unit localized at the distal end of the P-pilus from *E. coli* and the glycolipid galabiose,[19] suggesting adhesion mechanisms of different nature.

We propose that SpaC−SpaC recognition plays a role in mediating bacterial aggregation during host colonization as wild-type (WT) LGG cells readily aggregate in solution (25 ± 4 cells per aggregate), while a LGG mutant strain impaired in pili expression shows much lower tendency to form aggregates (see Figure 5c). This observation agrees well with the widely accepted notion that Gram-positive bacterial pili are engaged not only in bacterial−host interactions but also in bacterial aggregation through pili−pili bonds.[50] Also, the role of trans-protein interactions in cell−cell adhesion has been demonstrated at the single-molecule level in various organisms. In *M. tuberculosis*[31] and *C. albicans*,[37−40] trans-interactions between adhesins play a key role in cell−cell aggregation. Adhesion of endothelial cells is mediated by trans-interactions between cadherins.[48] Finally, the occurrence of SpaC homophilic recognition could explain the ability of LGG pili to form two-dimensional assemblies on solid surfaces.[51]

The molecular origin of the SpaC homophilic bonds is unclear. They could result from the presence of a stretch in the SpaC protein which is similar to the type A domain of the vWFA factor,[13] known to be involved in the formation of supramolecular structures.[52] As LGG pili might be glycosylated (work in progress) and SpaC may contribute to weak lectin-like activity by binding to heavily glycosylated mucus proteins,[13] it is also possible that lectin−glycan interactions take place. Lastly, nonspecific interactions like hydrophobic interactions could contribute, as well, as many bacterial pili are hydrophobic[53] and SpaC pilins are rich in hydrophobic residues.[13]

Molecular Details of the SpaC−Mucin Interaction. SpaC has been shown to bind to mucins,[13,23,54] a family of high molecular weight glycoconjugates with a rather complex composition which represents the main extracellular component of the intestinal mucosal layer. Although the SpaC−mucin interaction must play a pivotal role in establishing tight attachment between probiotics and their host, its molecular details are poorly understood. We therefore measured the binding forces between single Spac pilins (attached on AFM tips) and mucin (attached on model substrates) (Figure 2a,b). Figure 2c,d shows the force data collected between SpaC and mucin. In 17% of the force curves, we observed adhesion events, either single or multiple, that were well-described with a WLC model. They showed a mean adhesion force of 64 ± 20 pN (mean $\pm$ SD; $n = 600$ from three different tips and substrates; in case of multiple adhesion peaks, only the last event was considered) and a rupture length in the 10−200 nm range. Elongation distances are similar to those of the SpaC−SpaC interaction and seem rather short in view of the large size of mucin, an observation that is likely to originate from the multisite covalent attachment of the glycoconjugates on the substrate. The measured forces were specific as they were essentially abolished by performing the same experiment in the presence of anti-SpaC antibodies or with a BSA tip (Figure 2e). As expected for receptor−ligand bonds, adhesion forces increased linearly with the logarithm of the loading rate (Figure 2f). The slope ($f_\beta = 0.7 \pm 0.1 \times 10^{-11}$) and intercept ($r_{F=0} = 2.1 \pm 0.2 \times 10^{-10}$) enabled us to estimate the kinetic off-rate, $k_{off} = 0.05\ s^{-1}$. The slopes and intercepts (values $\pm$ errors) that we obtain for the SpaC−SpaC and SpaC−mucin systems suggest that these interactions have dissociation rates that are in the same range. The rapid dissociation of pilin−mucin bonds could be important for intestinal exploration and colonization, enabling pili to rapidly detach and bind new receptor sites. The mucin-binding capacity of the SpaC adhesin, measured here for the first time at the single-molecule level, is likely to play a role in the adhesion of other lactobacilli expressing pili.[55]

SpaC Shows Collagen-Binding Capacity. Several pilus-associated adhesins interact with extracellular matrix

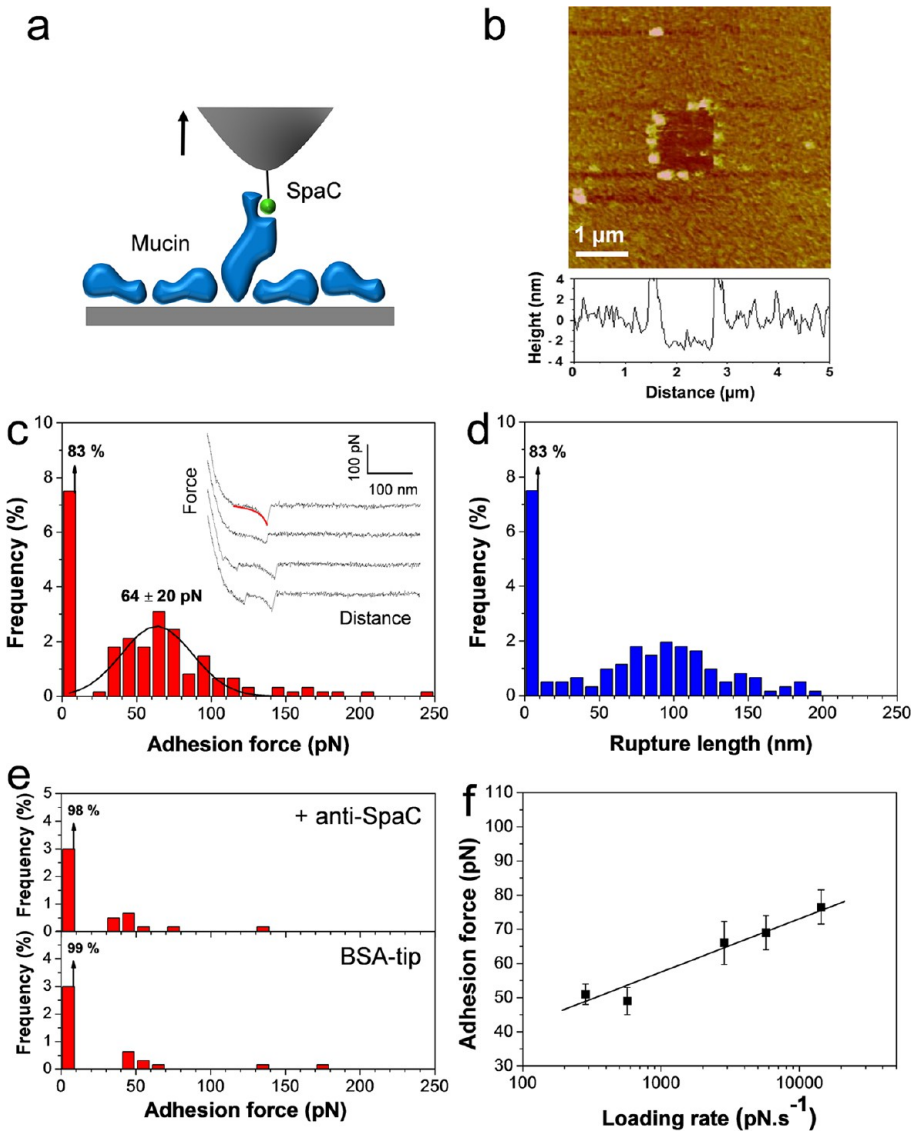

Figure 2. Strength and dynamics of the SpaC−mucin interaction. (a) Single SpaC−mucin interactions were explored by measuring the binding forces between a SpaC tip and mucin randomly attached on a gold substrate. (b) AFM image and vertical cross section confirming the presence of a 2.0 ± 0.4 nm thick mucin film on the surface. (c,d) Adhesion force histogram together with representative force curves (c) and rupture length histogram (d) obtained by recording force curves in buffer between a SpaC tip and a mucin substrate. All curves were obtained using a contact time of 100 ms, a maximum applied force of 250 pN, and approach and retraction speeds of 1000 nm/s. The black line is a Gaussian fit to the data. Force peaks were well-described by the worm-like-chain model (red line on top curve in c). The data shown correspond to 600 force curves obtained from three independent experiments. (e) Control experiments showing a dramatic reduction of adhesion frequency when force measurements were performed in the presence of free anti-SpaC antibodies (top, *n* = 600) or with a BSA-coated tip (bottom, *n* = 600). (f) Plot of the SpaC−mucin adhesion force as a function of the logarithm of the loading rate applied during retraction, while keeping constant the approach speed (1000 nm/s). Each data point in this plot represents the mean ± SEM (*n* = 200 force curves). A similar plot was obtained in a duplicate experiment using different tip and substrate.

(ECM) proteins like fibronectin and collagen,[56−60] including those from *Lactobacillus* strains.[61] In LGG, SpaCBA pili, and not MabA,[62] appear to mediate strong ECM-binding capacity.[14] Therefore, we measured the binding forces between single SpaC pilins and collagen (Figure 3a,b). In 15% of the curves, we observed adhesion forces of 75 ± 28 pN (mean ± SD; *n* = 600 from three different tips and substrates; in case of multiple adhesion peaks, only the last event was considered) with rupture lengths in the 50−200 nm range (Figure 3c,d), the adhesion peaks being well-fitted with a WLC model. The extended rupture lengths may be easily explained by the filamentous structure of the collagen molecule. Adhesive forces were less frequent and smaller in the presence of anti-SpaC antibodies (Figure 3e, top), suggesting that a substantial fraction of the 75 pN forces were specific. Substantial binding was observed with the BSA tip, indicating that BSA was interacting with collagen (Figure 3e, bottom). Consistent with specific bonds, SpaC−collagen forces increased linearly with the logarithm of the loading rate (Figure 3f). From the slope (f_β = $0.8 \pm 0.1 \times 10^{-11}$) and intercept ($r_{F=0} = 2.4 \pm 0.2 \times 10^{-10}$)

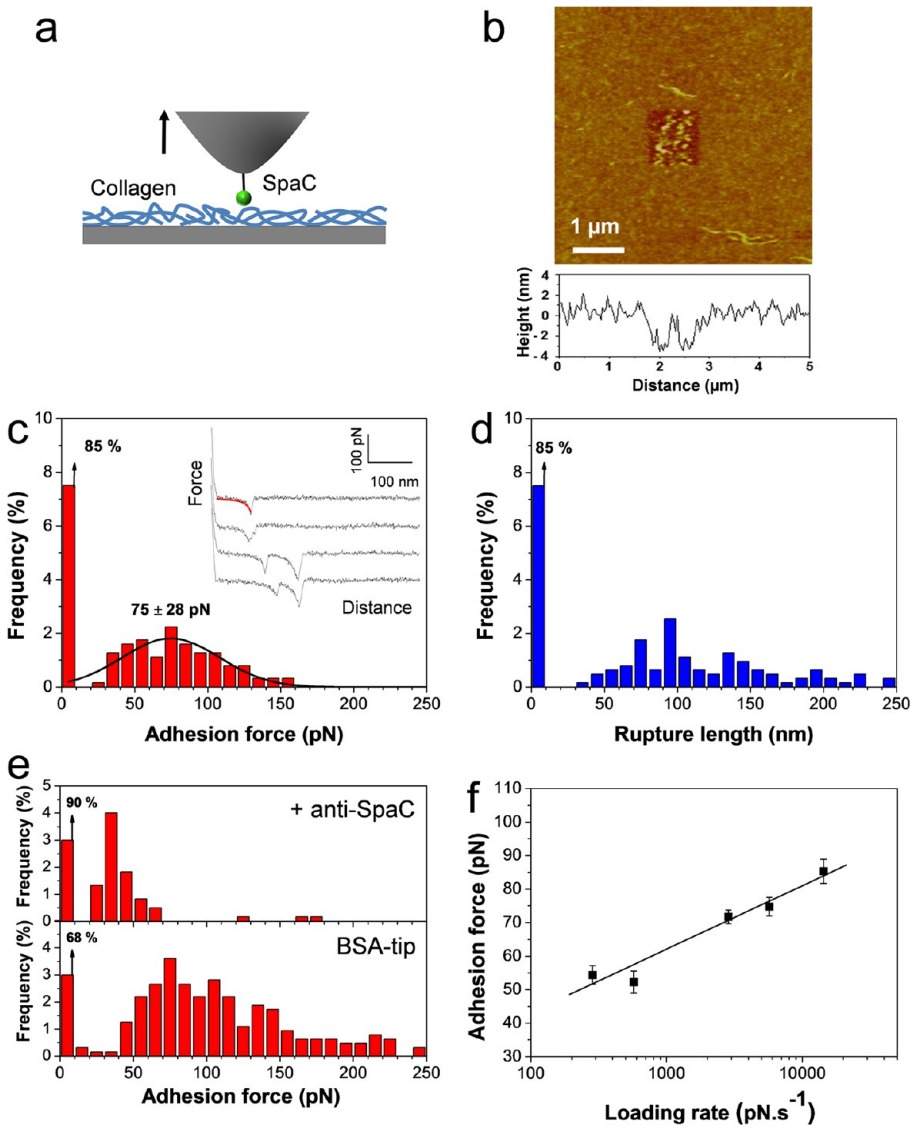

Figure 3. Strength and dynamics of the SpaC−collagen interaction. (a) Binding forces between a SpaC tip and collagen randomly attached on a gold substrate. (b) AFM confirmed the presence of a 2.0 ± 0.5 nm thick collagen film on the substrate. (c,d) Adhesion force histogram together with representative force curves (c) and rupture length histogram (d) obtained by recording force curves in buffer between a SpaC tip and a collagen substrate. All curves were obtained using a contact time of 100 ms, a maximum applied force of 250 pN, and approach and retraction speeds of 1000 nm/s. The black line is a Gaussian fit to the data. Force peaks were well-described by the worm-like-chain model (red line on top curve in c). The data shown correspond to 600 force curves obtained from three independent experiments. (e) Control experiments in which force measurements were performed in the presence of free anti-SpaC antibodies (top, *n* = 600) or with a BSA-coated tip (bottom, *n* = 600). (f) Plot of the SpaC−collagen adhesion force as a function of the logarithm of the loading rate applied during retraction, while keeping constant the approach speed (1000 nm/s). Each data point in this plot represents the mean ± SEM (*n* = 200 force curves). Similar plot was obtained in a duplicate experiment using different tip and substrate.

of the plot, we found a k_{off} value of 0.08 s^{-1}, thus in the range of the SpaC−mucin value. Again, this suggests that fast SpaC−collagen dissociation may help pili to rapidly detach and rebind to host sites. The *in vivo* significance of this collagen-binding capacity is not clear yet as ECM components are thought to be available for interaction only after disruption of the epithelial barrier.[61]

SpaC Mediates Zipper-like Adhesion. At first glance, our finding that SpaC exhibits broad specificity and fast dissociation seems surprising as bacterial pili are generally considered as strong adhesion structures. However, we must consider that, like other Gram-positive bacterial adhesins, SpaC is abundant and localized not only at the pilus tip but also along its length. Indeed, electron microscopy analyses revealed that SpaC pilins are found randomly along the whole pilus, at numbers nearly equaling those of SpaA, while SpaB pilins are essentially found at the pilus base.[23] This organization favors a zipper-like adhesion model involving multiple SpaC distributed along the pilus shaft. Such zipper mechanism has been suggested for Gram-positive bacterial pili[50] but, to our knowledge, never demonstrated or quantified.

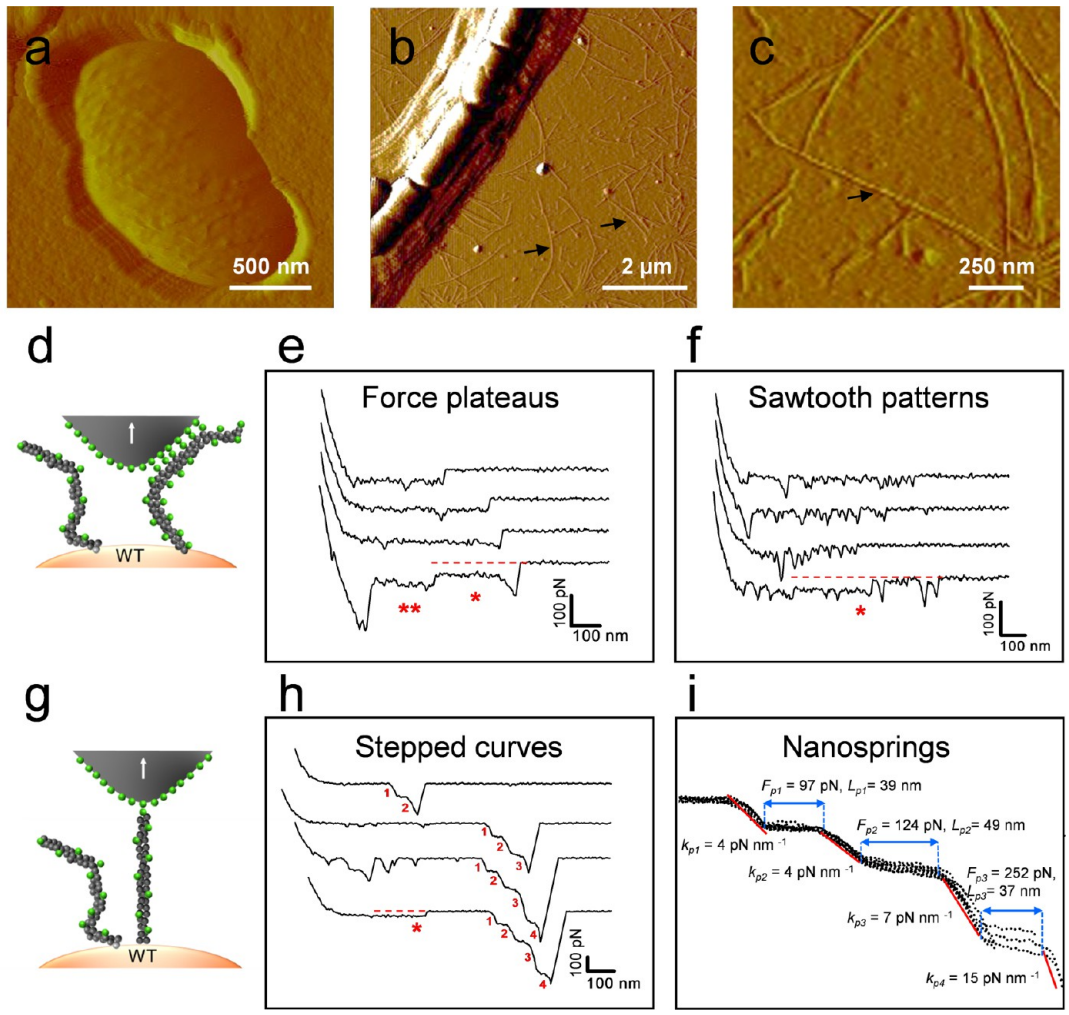

Figure 4. Measuring the nanomechanics of single pili on live cells. (a–c) AFM visualizes LGG pili in air but not in liquid: (a) deflection image of a LGG bacterium trapped in a porous membrane, recorded in buffer, showing a surface morphology devoid of pili; (b) deflection image of LGG bacteria adsorbed on mica and recorded in air, revealing numerous pili around the cells (arrows); (c) high-resolution image of pili showing helical spring-like structures (arrow). (d–f) LGG pili mediate zipper-like adhesion: (d) pulling single pili with a SpaC tip leads to the sequential detachment of multiple SpaC–SpaC bonds; as a result, (e) a notable fraction of the curves showed constant force plateaus, sometimes superimposed onto one another (see ** symbol), while (f) other curves showed multiple force peaks forming sawtooth patterns, sometimes superimposed onto constant force plateaus (see * symbol). Dashed lines on the bottom curves represent zero force lines. (g–i) LGG pili behave as nanosprings: (g) stretching pili into extended conformations with a SpaC tip; (h) a substantial fraction of force curves revealed single adhesion force peaks with linear, spring-like shapes and characteristic steps; red numbers correspond to linear segments of increasing slopes; (i) superimposition of 10 curves showing that spring-like properties are highly reproducible and can be quantified. The k_p values represent the force-dependent pilus spring constants, while the F_p and L_p values correspond to the force and length of the constant force steps. The curves were obtained using a contact time of 100 ms, a maximum applied force of 250 pN, and approach and retraction speeds of 1000 nm/s. Similar data were obtained using three different tips and three different cell cultures.

To explore whether SpaC is engaged in zipper-like adhesion, we measured the forces between an AFM tip bearing SpaC pilins and pili on living LGG bacteria (Figure 4). We first confirmed the presence of pili on the cell surface by imaging WT LGG bacteria with a silicon nitride tip (Figure 4a–c). Consistent with earlier work,[51] pili could never be observed using AFM in liquid, indicating they were too flexible and mobile to be visualized (Figure 4a). By contrast, bacteria imaged in air were decorated with numerous pili displaying an average length of 1.0 ± 0.3 μm and average diameter of 5.0 ± 1 nm (Figure 4b). At high resolution, some pili featured a helical structure with 20–50 nm repeats (Figure 4c), suggesting spring-like properties. As these structural features were repeatedly observed on some pili and were not dependent on the scanning direction, they are likely to reflect actual helical structures rather than imaging artifacts.

We then recorded multiple force–distance curves between a SpaC tip and a WT LGG cell in buffer (Figure 4d). Three remarkable adhesion signatures were detected, that is, constant force plateaus (3%, Figure 4e), sawtooth patterns composed of multiple small force peaks (36%, Figure 4f), sometimes superimposed to

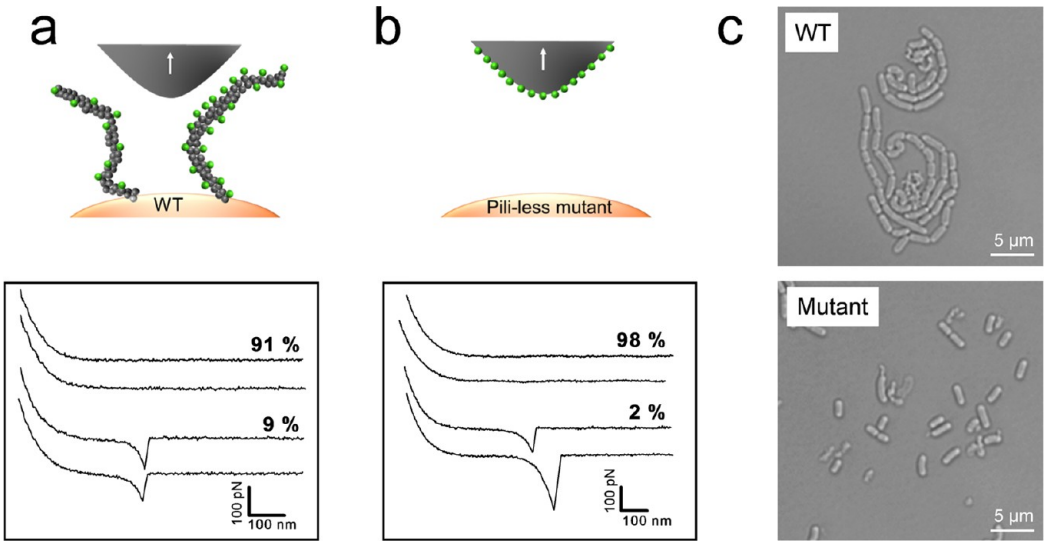

Figure 5. Control experiments demonstrate that zipper and spring force responses are specific to pili. (a,b) Representative force−distance curves recorded in buffer between a nonfunctionalized tip and a wild-type (WT) LGG bacterium (a) and between an LGG mutant strain impaired in pili expression and a SpaC tip (b). Both conditions lead to the complete disappearance of plateau, sawtooth, and linear signatures. (c) Unlike WT cells (top), pili-deficient mutant cells do not aggregate in solution (bottom).

constant force plateaus, and single large adhesion force peaks with linear shape and characteristic horizontal force steps (24%, Figure 4h). The remaining fraction of adhesive curves showed elastic force peaks of 30−300 pN magnitude.

Several observations suggest that the observed force plateaus represent the mechanical response of a molecular zipper. First, the magnitude of the plateau force was 46 ± 4 pN (mean ± SD; n = 30 plateaus) and occasionally 98 ± 4 pN (Figure 4e, bottom curve), suggesting that each plateau force was a multiple of a ~50 pN unit force. Given the accuracy of our measurements, this value is not too different from the ~60 pN force measured for the homophilic SpaC−SpaC interaction on solid substrates (Figure 1), suggesting that plateau forces may involve the sequential rupture of multiple SpaC−SpaC bonds. The low unbinding forces observed for pili, compared to purified pilins, could reflect the influence of the complex environment of the pilus; for example, the flexible nature of pili may lower the loading rate actually applied to the SpaC molecules. Second, the length of the force plateaus, 488 ± 168 nm, corresponds to half the length of the pili. Third, force plateaus were never observed between a WT cell and a bare silicon nitride tip (Figure 5a), suggesting strongly that they involve specific bonds between SpaC pilins on the tip and pili. Fourth, they were not observed when probing cells from an LGG mutant strain impaired in pili expression with a SpaC tip (Figure 5b), indicating that these force responses are associated with pili. Fifth, SpaC pilins are known to be abundant along the full pilus length,[23] an organization which strongly favors the formation of a molecular zipper (see cartoon in Figure 4d). Sixth, our force plateaus are reminiscent of the signatures measured for the mechanical unzipping of β-sheet interactions in pathological[63] and functional[39] amyloids and for the continuous desorption of polymer chains adsorbed on solid substrates.[64] Pulling on weakly adsorbed polymer chains yields constant force plateaus when bond dissociation is faster than the pulling rate.[64] As the dissociation rate of the SpaC−SpaC bond is likely to be faster than the time scale of our experiment, stretched pili may be viewed as strings of SpaC pilins continuously detaching from the SpaC tip. In summary, our experiments reveal that the LGG pilus mediates zipper-like interactions involving multiple SpaC adhesins distributed along the pilus. The term "unzipping" refers to a specific pulling geometry in the single-molecule field. The so-called "zipper mode" is exclusively used for disrupting multiple interactions one-by-one along the applied force such as when pulling dsDNA on the 3′ and 5′ ends.[65] In contrast, in the so-called "shear mode", all interactions are loaded in parallel and rupture cooperatively, like when pulling dsDNA at both 3′ ends. Due to the very complex and dynamic environment of pili—in terms of density, orientation, mobility, and lateral interactions—we cannot fully control the pulling geometry (zipper mode *vs* shear mode) in our live cell experiments.

How about the origin of the sawtooth patterns (Figure 4f)? We believe these multiple force peaks also captured the sequential detachment of multiple SpaC as (i) they were never observed with silicon nitride tips or with pili-less mutant cells (Figure 5), and (ii) they featured average forces (32 ± 9 pN) and rupture lengths (704 ± 110 nm) that were in the range of those of the force plateaus (Figure 4f). Hence, each discrete peak would correspond to the detachment of

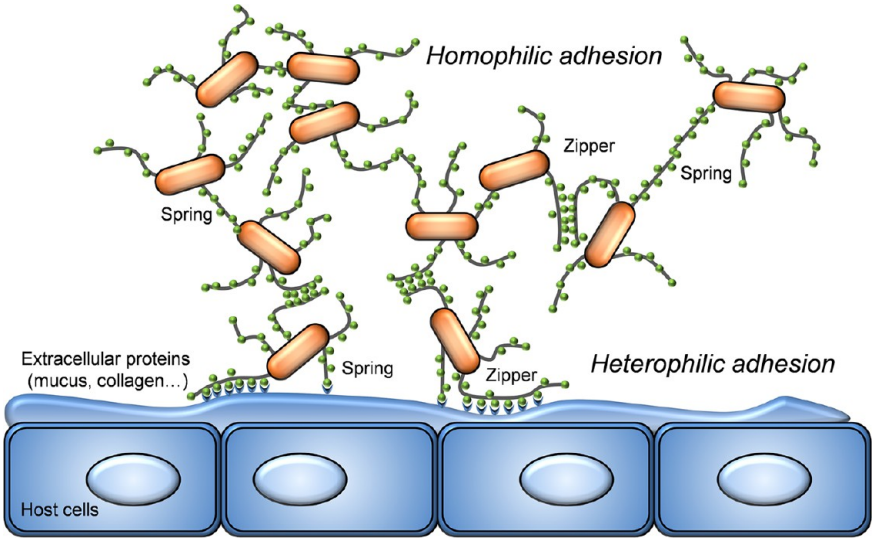

Figure 6. Molecular mechanism of pili-mediated adhesion. SpaC specifically binds to mucin and collagen, two major extracellular components of host epithelial layers, and is also engaged in homophilic adhesion. While the SpaC molecular zipper provides a powerful mechanism to strengthen bacterial−host and bacterial−bacterial adhesion, the spring properties of pili enable the bacteria to withstand high shear stress.

a single SpaC bond. Such behavior is expected when the number of SpaC bonds between pilus and tip is low, thus when the density of pilins along the tip is low. In the future, it would be interesting to confirm that the appearance of force plateaus *versus* sawtooth patterns may indeed be explained by different numbers of SpaC bonds formed between pilus and tip by immobilizing different amounts of SpaC to the tip through the use of different surface chemistries. Also, further experiments are needed to establish whether plateau and sawtooth patterns reflect some structural heterogeneity in the pili population. Nevertheless, these two mechanisms are likely to fulfill the same function, that is, increasing the strength and lifetime of bacterial cell surface interactions.

LGG Pilus Behaves as a Nanospring. Another key finding is the presence of large adhesion force peaks with linear shapes and constant force steps (Figure 4g−i), sometimes preceded with constant force plateaus (Figure 4h, bottom curve). Again, these profiles are attributed to the specific binding and pulling of LGG pili as they were never observed with silicon nitride tips or with pili-less mutant cells (Figure 5). As expected, linear regions could not be fitted with a WLC model, indicating they did not correspond to the force-induced unfolding of protein structures. Rather, force was directly proportional to extension, meaning that the stretched pili behaved as Hookean springs. Superimposition of multiple force profiles documented a high reproducibility (Figure 4i), thus supporting the notion that they reflect an intrinsic mechanical property of single pili rather than some random, poorly controlled processes, such as desorption of multiple pili from the tip. Upon increasing the applied force, up to three consecutive constant force steps were observed (blue arrows in Figure 4i), followed by linear segments of increasing slopes (red lines in Figure 4i), suggesting stiffening of the pulled filaments. These stepwise interactions ruptured at relatively high forces (up to 250−300 pN), clearly stronger than that of individual SpaC−SpaC interactions. We therefore suggest that, in the high force regime, a few remaining SpaC interactions are loaded in parallel (shear mode), thus allowing the tip to stretch the pilus up to several hundreds of piconewton. This model does not contradict the unzipping model occurring in the low force regime.

To further quantify the mechanical behavior of individual pili, we estimated their spring constant in the different loading regimes (Figure 4i). The experimental system corresponds to two linear springs in series, one being the AFM cantilever (k_c) and the other the pili spring constant (k_p). Using the slope (s) of the linear portion of the raw deflection *versus* piezo displacement curves and the following equation, $k_p = (k_c \times s)/(1 - s)$, we found that the pilus spring constants estimated for the different regimes were $k_{p1} = 4.3 \pm 0.5$ pN nm^{-1}, $k_{p2} = 3.6 \pm 0.2$ pN nm^{-1}, $k_{p3} = 7.1 \pm 0.4$ pN nm^{-1}, and $k_{p4} = 15.1 \pm 0.9$ pN nm^{-1}. Notably, the characteristics of the stepwise transitions were highly reproducible, that is, step force values of $F_{p1} = 97 \pm 4$ pN, $F_{p2} = 124 \pm 11$ pN, $F_{p3} = 252 \pm 26$ pN, and step length values of $L_{p1} = 39 \pm 3$ nm, $L_{p2} = 49 \pm 4$ nm, and $L_{p3} = 37 \pm 1$ nm. Given the high reproducibility of these features, we suggest they reflect an intrinsic mechanical response of the pilus, that is, force-induced structural changes within the pilus leading to stiffer conformations.

Our finding that the LGG pilus functions as a spring agrees well with earlier structural and single-molecule data. Gram-positive bacterial pili exhibit internal isopeptide bonds not found in other proteins and

believed to stabilize the pilus mechanical properties.[27] At the single pilin level, AFM revealed that Gram-positive bacterial pilins cannot be unfolded even by large mechanical forces, meaning they are completely inextensible.[44] Spring-like properties of LGG pili are also supported by our AFM images showing that some of them have a helical spring-like structure (Figure 4c). We expect that the spring behavior of the LGG pilus is of biological significance as it may help bacteria to withstand physiological shear forces while being engaged in bacterial−host and bacterial−bacterial interactions.

Collectively, our results demonstrate that the LGG pilus exhibits two striking mechanical responses (*i.e.*, zipper-like adhesion at low force and nanospring behavior at high force). These biophysical properties largely differ from those of the widely investigated Gram-negative pili. As Gram-positive bacterial pili are formed by covalent polymerization and are stabilized by internal isopeptide bonds,[25,27] they are ideally suited to possess zipper-like and spring-like functions. By contrast, pili from Gram-negative bacteria are formed by noncovalent interactions between pilin subunits,[66] explaining why they readily elongate under force as a result of the unfolding of their helical quaternary structure.[17−19,22] This elongation is believed to help bacteria to redistribute external forces to multiple pili, thereby enabling them to withstand shear forces. In addition, type IV pili from Gram-negative bacteria like *Neisseria gonorrheae* are able to exert retractile forces involved in twitching motility and host cell adhesion, presumably through filament disassembly into the inner membrane.[67] Cooperative retraction of bundled pili can generate forces in the nanonewton range that could be critical for bacterial surface interactions.[68] Another feature of Gram-negative bacterial pili is their ability to mediate catch bonds, for example, receptor−ligand bonds that are strengthened by mechanical force owing to an allosteric switch.[20,21] A prominent example is the fimbrial adhesive protein FimH from *E. coli*, which mediates weak adhesion at low flow but strong adhesion at high flow.[20,21] These observations suggest that pili from Gram-negative and Gram-positive bacteria have developed very different adhesion strategies.

CONCLUSIONS

Understanding and controlling bacterial−host interactions in the context of human health (probiotics, pathogens) requires elucidation of the molecular mechanisms by which bacteria attach to their host. In the past years, single-molecule techniques have provided new insights into the adhesive and mechanical properties of Gram-negative bacterial pili, thereby explaining how these structures are used to strengthen adhesion and resist mechanical stress.[16−22,67,68] By contrast, little is known about the nanomechanics of Gram-positive bacterial pili. Our single-molecule experiments demonstrate that LGG pili exhibit adhesive and mechanical properties that clearly differ from those observed in Gram-negative bacteria. Our main findings are as follows: (i) at the single-molecule level, SpaC mediates homophilic (SpaC−SpaC) and heterophilic (SpaC−mucin, SpaC−collagen) interactions of similar adhesive strength; (ii) the fast dissociation rate of these interactions could be important for intestinal colonization, enabling pili to rapidly detach and bind new receptor sites; (iii) the LGG pilus mediates SpaC zipper-like interactions involving multiple adhesins distributed along the pilus (zipper mode rupture at low force); (iv) it also functions as a nanospring capable to withstand large mechanical loads (shear mode rupture at high force) and showing stepwise transitions presumably reflecting structural changes.

We expect that the broad binding specificity, zipper-like interactions, and spring-like properties of LGG pili may have an important functional role in strengthening bacterial−host and bacterial−bacterial interactions in the intestinal environment (Figure 6). Following initial contact, multisite attachment down the pilus length would pull the bacteria closer to the host cells, leading to firm and intimate contact. Then, pilus-mediated bacterial aggregation would contribute to strengthen colonization and biofilm formation. During these processes, the pilus spring behavior may help the bacteria to withstand physiological shear forces. Increasing the external force would lead to structural transitions, resulting in stiffer pilus conformations. Altogether, these mechanical properties would explain the prolonged intestinal residency time observed for LGG compared to that of nonpiliated lactobacilli.[13,23] In addition to providing new insights into the molecular mechanisms of pili-mediated adhesion, our experiments may be of biomedical interest for the design of molecules that promote (probiotics) or inhibit (pathogens) bacterial adhesion.

METHODS

Microorganisms and Cultures. LGG (ATCC 53103) wild-type and the pili-deficient mutant CMPG5357[14] were grown in de Man−Rogosa−Sharpe (MRS) broth (Difco) up to the midexponential phase. Bacterial cells stored in MRS broth with 25% (v/v) glycerol at −80 °C were revived by streaking on MRS agar and allowed to grow at 37 °C for 48 h. Preculture was initiated by inoculating a single colony of bacteria into 10 mL of MRS broth. This preculture was used to inoculate fresh MRS broth, and the cells were kept at 37 °C for 8 h (when the culture reached optical density of 0.8−1.0 at 595 nm). Cells were harvested by centrifuging the culture at 5000*g* for 2 min. The supernatant was discarded, and the pellet was resuspended in 10 mL of Tris buffer. For AFM analysis, the cell suspension was diluted by 50% in the buffer and was filtered under pressure through isopore membranes (Millipore, Billerica, MA) with pore diameter comparable to cell size (1.2 μm).[69] The membrane was rinsed in four baths of the buffer, and 1 cm × 1 cm pieces were cut and attached to an AFM sample puck using double-sided adhesive tape.

Preparation of SpaC Pilin Monomers. The *spaC* (*LGG_00404*) gene, excluding the region encoding the N-terminal signal peptide and the C-terminal cell wall sorting signal, was recombinantly expressed in *E. coli* and then purified as previously described.[13]

Preparation of SpaC-Modified Tips. AFM tips were functionalized with SpaC proteins in a random orientation using ~6 nm long PEG-benzaldehyde linkers as described by Ebner *et al.*[70] Cantilevers were washed in three successive baths of chloroform followed by rinsing with ethanol. The tips were dried with N_2 and placed in a UV-ozone cleaner for 30 min, immersed overnight in an ethanolamine solution (3.3 g of ethanolamine dissolved in 6 mL of DMSO), then washed three times with DMSO and twice with ethanol, and dried with N_2. The ethanolamine-coated cantilevers were immersed for 2 h in a solution prepared by mixing 1 mg of acetal-PEG-NHS dissolved in 0.5 mL of chloroform with 10 μL of triethylamine, then washed with chloroform, and dried with N_2. Cantilevers were then immersed in a 1% citric acid solution for 10 min, washed in Milli-Q water, and then covered with a 200 μL droplet of a Tris (pH 7.4) solution containing the protein (0.1 mg/mL) to which 2 μL of a 1 M $NaCNBH_3$ solution was added. After 50 min, cantilevers were incubated with 5 μL of a 1 M ethanolamine solution in order to passivate unreacted aldehyde groups and then washed with and stored in buffer. For storage beyond 24 h, the tips were kept in Tris containing sodium nitride to prevent oxidation damage to the protein. For control experiments, tips functionalized with BSA were prepared using the same procedure.

Preparation of SpaC-, Mucin-, and Collagen-Modified Surfaces. SpaC, mucin, and collagen were covalently immobilized, in a random orientation, onto self-assembled monolayers (SAMs) of carboxyl-terminated alkanethiols. Silicon wafers (Siltronix, France) were coated by thermal evaporation with a 5 nm thick Cr layer followed by a 30 nm thick Au layer, yielding gold surfaces with ~1 nm roughness. Gold surfaces were immersed overnight in ethanol solutions containing 1 mM of $HS(CH_2)_{15}COOH$ (16-mercaptohexadecanoic acid) and $HS(CH_2)_{11}OH$ (11-mercapto-1-undecanol) (0.1:0.9) (Sigma) and then rinsed with ethanol. Sonication was briefly applied to remove alkanethiol aggregates that may have been adsorbed. The SAMs were immersed for 30 min in a solution containing 20 mg/mL *N*-hydroxysuccinimide (NHS) (Sigma) and 50 mg/mL 1-ethyl-3-(3-dimethylaminopropyl)carbodiimide (EDC) (Sigma) and rinsed with water. The activated surfaces were then incubated with 0.1 mg/mL SpaC protein, 10 mg/mL mucin (mucin from porcine stomach, type II, Sigma), or 25 mg/mL collagen (type I from calf skin, Sigma) in Tris for either 2 h (SpaC, mucin) or 1 h (collagen), followed by rinsing and storage in Tris. All surfaces were freshly prepared and used the same day.

AFM Measurements. AFM measurements were performed at room temperature (20 °C) in Tris buffer (pH 7.4) using a Nanoscope V Multimode AFM from Bruker Corporation (Santa Barbara, CA) and microfabricated Si_3N_4 cantilevers with a nominal spring constant of ~0.01 N/m (MSCT from Bruker Corporation). Unless stated otherwise, all force curves were obtained using a contact time of ~100 ms, a maximum applied force of 250 pN, and approach and retraction speeds of 1000 nm/s. For experiments on purified proteins with increasing force loads, the retraction speed was varied between 100 and 5000 nm s^{-1}. To account for the flexibility of the biomolecules, loading rates (pN s^{-1}) were estimated by multiplying the tip retraction velocity (nm s^{-1}) by the slope of the rupture peaks (pN nm^{-1}). Antibody blocking experiments were performed by addition of a ~0.1 mg/mL solution of a previously produced SpaC antiserum.[13] For live cell experiments, the sample was first scanned with a silicon nitride tip to localize a single LGG cell. Then, the tip was changed with a functionalized tip in order to record force maps on 500 nm × 500 nm areas over the cell surface (for details, see ref 69). The spring constants of the cantilevers were measured using the thermal noise method.

Conflict of Interest: The authors declare no competing financial interest.

Acknowledgment. Work in the Y.F.D. team was supported by the National Foundation for Scientific Research (FNRS), the Foundation for Training in Industrial and Agricultural Research (FRIA), the Université catholique de Louvain (Fonds Spéciaux de Recherche), the Federal Office for Scientific, Technical and Cultural Affairs (Interuniversity Poles of Attraction Programme), and the Research Department of the Communauté française de Belgique (Concerted Research Action). Y.F.D. and D.A. are Senior Research Associate and Postdoctoral Researcher of the FRS-FNRS. P.T. is supported by a fellowship from Erasmus Mundus External Cooperation Window Lot 13. Work at KU Leuven was supported by the BOF-Programme financing (spokesman Jan Balzarini). Work performed by the A.P. team (University of Helsinki) was financed by an Academy of Finland general research grant (118165) and by the Academy of Finland-funded Center of Excellence in Microbial Food Safety (CoE-MiFoSa) research program (141140). Outi Lyytinen (University of Helsinki) is thanked for technical assistance with protein purification.

REFERENCES AND NOTES

1. Madsen, K.; Cornish, A.; Soper, P.; McKaigney, C.; Jijon, H.; Yachimec, C.; Doyle, J.; Jewell, L.; De Simone, C. Probiotic Bacteria Enhance Murine and Human Intestinal Epithelial Barrier Function. *Gastroenterology* **2001**, *121*, 580–591.
2. Lee, Y. K.; Puong, K. Y.; Ouwehand, A. C.; Salminen, S. Displacement of Bacterial Pathogens From Mucus and Caco-2 Cell Surface by *Lactobacilli*. *J. Med. Microbiol.* **2003**, *52*, 925–930.
3. Servin, A. L. Antagonistic Activities of *Lactobacilli* and *Bifidobacteria* Against Microbial Pathogens. *FEMS Microbiol. Rev.* **2004**, *28*, 405–440.
4. Corthésy, B.; Gaskins, H. R.; Mercenier, A. Cross-Talk between Probiotic Bacteria and the Host Immune System. *J. Nutr.* **2007**, *137*, 781S–790S.
5. Yan, F.; Cao, H.; Cover, T. L.; Whitehead, R.; Washington, M. K.; Polk, D. B. Soluble Proteins Produced by Probiotic Bacteria Regulate Intestinal Epithelial Cell Survival and Growth. *Gastroenterology* **2007**, *132*, 562–575.
6. Lebeer, S.; Vanderleyden, J.; De Keersmaecker, S. C. Adaptation Factors of the Probiotic *Lactobacillus rhamnosus* GG. *Benefic. Microbes* **2010**, *1*, 335–342.
7. Bron, P. A.; Van Baarlen, P.; Kleerebezem, M. Emerging Molecular Insights into the Interaction between Probiotics and the Host Intestinal Mucosa. *Nat. Rev. Microbiol.* **2012**, *10*, 66–78.
8. Borchers, A. T.; Selmi, C.; Meyers, F. J.; Keen, C. L.; Gershwin, M. E. Probiotics and Immunity. *J. Gastroenterol.* **2009**, *44*, 26–46.
9. Amdekar, S.; Dwivedi, D.; Roy, P.; Kushwah, S.; Singh, V. Probiotics: Multifarious Oral Vaccine Against Infectious Traumas. *FEMS Immunol. Med. Microbiol.* **2010**, *58*, 299–306.
10. Kirjavainen, P. V.; Ouwehand, A. C.; Isolauri, E.; Salminen, S. J. The Ability of Probiotic Bacteria To Bind to Human Intestinal Mucus. *FEMS Microbiol. Lett.* **1998**, *167*, 185–189.
11. Salminen, S.; Nybom, S.; Meriluoto, J.; Collado, M. C.; Vesterlund, S.; El-Nezami, H. Interaction of Probiotics and Pathogens—Benefits to Human Health? *Curr. Opin. Biotechnol.* **2010**, *21*, 157–167.
12. Dicks, L. M.; Botes, M. Probiotic Lactic Acid Bacteria in the Gastro-intestinal Tract: Health Benefits, Safety and Mode of Action. *Benefic. Microbes* **2010**, *1*, 11–29.
13. Kankainen, M.; Paulin, L.; Tynkkynen, S.; von Ossowski, I.; Reunanen, J.; Partanen, P.; Satokari, R.; Vesterlund, S.; Hendrickx, A. P. A.; Lebeer, S.; *et al.* Comparative Genomic Analysis of *Lactobacillus rhamnosus* GG Reveals Pili Containing a Human-Mucus Binding Protein. *Proc. Natl. Acad. Sci. U.S.A.* **2009**, *106*, 17193–17198.
14. Lebeer, S.; Claes, I.; Tytgat, H. L. P.; Verhoeven, T. L. A.; Marien, E.; von Ossowski, I.; Reunanen, J.; Palva, A.; de Vos, W. M.; De Keersmaecker, S. C. J.; *et al.* Functional Analysis of *Lactobacillus rhamnosus* GG Pili in Relation to Adhesion and Immunomodulatory Interactions with Intestinal Epithelial Cells. *Appl. Environ. Microbiol.* **2012**, *78*, 185–193.

15. Maier, B.; Potter, L.; So, M.; Seifert, H. S.; Sheetz, M. P. Single Pilus Motor Forces Exceed 100 pN. *Proc. Natl. Acad. Sci. U.S.A.* **2002**, *99*, 16012–16017.
16. Andersson, M.; Fällman, E.; Uhlin, B. E.; Axner, O. Dynamic Force Spectroscopy of *E. coli* P Pili. *Biophys. J.* **2006**, *91*, 2717–2725.
17. Miller, E.; Garcia, T.; Hultgren, S.; Oberhauser, A. F. The Mechanical Properties of *E. coli* Type 1 Pili Measured by Atomic Force Microscopy Techniques. *Biophys. J.* **2006**, *91*, 3848–3856.
18. Touhami, A.; Jericho, M. H.; Boyd, J. M.; Beveridge, T. J. Nanoscale Characterization and Determination of Adhesion Forces of *Pseudomonas aeruginosa* Pili by Using Atomic Force Microscopy. *J. Bacteriol.* **2006**, *188*, 370–377.
19. Lugmaier, R. A.; Schedin, S.; Kühner, F.; Benoit, M. Dynamic Restacking of *Escherichia coli* P-Pili. *Eur. Biophys. J.* **2008**, *37*, 111–120.
20. Yakovenko, O.; Sharma, S.; Forero, M.; Tchesnokova, V.; Aprikian, P.; Kidd, B.; Mach, A.; Vogel, V.; Sokurenko, E.; Thomas, W. E. FimH Forms Catch Bonds That Are Enhanced by Mechanical Force Due to Allosteric Regulation. *J. Biol. Chem.* **2008**, *283*, 11596–11605.
21. Sokurenko, E. V.; Vogel, V.; Thomas, W. E. Catch-Bond Mechanism of Force-Enhanced Adhesion: Counterintuitive, Elusive, but ... Widespread? *Cell Host Microbe* **2008**, *4*, 314–323.
22. Castelain, M.; Sjöström, A. E.; Fällman, E.; Uhlin, B. E.; Andersson, M. Unfolding and Refolding Properties of S Pili on Extraintestinal Pathogenic *Escherichia coli*. *Eur. Biophys. J.* **2010**, *39*, 1105–1115.
23. Reunanen, J.; von Ossowski, I.; Hendrickx, A. P. A.; Palva, A.; de Vosa, W. M. Characterization of the SpaCBA Pilus Fibers in the Probiotic *Lactobacillus rhamnosus* GG. *Appl. Environ. Microbiol.* **2012**, *78*, 2337–2344.
24. Deivanayagam, C. C. S.; Rich, R. L.; Danthuluri, S.; Owens, R. T.; Patti, J. M.; Höök, M.; DeLucas, L. J.; Narayana, S. V. L Crystallization and Preliminary X-ray Analysis of B-Domain Fragments of a *Staphylococcus aureus* Collagen-Binding Protein. *Acta Crystallogr. D* **1999**, *55*, 525–527.
25. Kang, H. J.; Baker, E. N. Structure and Assembly of Gram-Positive Bacterial Pili: Unique Covalent Polymers. *Curr. Opin. Struct. Biol.* **2012**, *22*, 200–207.
26. Kang, H. J.; Paterson, N. G.; Gaspar, A. H.; Ton-That, H.; Baker, E. N. The *Corynebacterium diphtheriae* Shaft Pilin SpaA Is Built of Tandem Ig-like Modules with Stabilizing Isopeptide and Disulfide Bonds. *Proc. Natl. Acad. Sci. U.S.A.* **2009**, *106*, 16967–16971.
27. Kang, H. J.; Coulibaly, F.; Clow, F.; Proft, T.; Baker, E. N. Stabilizing Isopeptide Bonds Revealed in Gram-Positive Bacterial Pilus Structure. *Science* **2007**, *318*, 1625–1628.
28. Pointon, J. A.; Smith, W. D.; Saalbach, G.; Crow, A.; Kehoe, M. A.; Banfield, M. J. A Highly Unusual Thioester Bond in a Pilus Adhesin Is Required for Efficient Host Cell Interaction. *J. Biol. Chem.* **2010**, *285*, 33858–33866.
29. Izoré, T.; Contreras-Martel, C.; El Mortaji, L.; Manzano, C.; Terrasse, R.; Vernet, T.; Di Guilmi, A. M.; Dessen, A. Structural Basis of Host Cell Recognition by the Pilus Adhesin from *Streptococcus pneumoniae*. *Structure* **2010**, *18*, 106–115.
30. Dupres, V.; Menozzi, F. D.; Locht, C.; Clare, B. H.; Abbott, N. L.; Cuenot, S.; Bompard, C.; Raze, D.; Dufrêne, Y. F. Nanoscale Mapping and Functional Analysis of Individual Adhesins on Living Bacteria. *Nat. Methods* **2005**, *2*, 515–520.
31. Verbelen, C.; Raze, D.; Dewitte, F.; Locht, C.; Dufrêne, Y. F. Single-Molecule Force Spectroscopy of Mycobacterial Adhesin–Adhesin Interactions. *J. Bacteriol.* **2007**, *189*, 8801–8806.
32. Verbelen, C.; Dupres, V.; Raze, D.; Bompard, C.; Locht, C.; Dufrêne, Y. F. Interaction of the Mycobacterial Heparin-Binding Hemagglutinin with Actin, as Evidenced by Single-Molecule Force Spectroscopy. *J. Bacteriol.* **2008**, *190*, 7614–7620.
33. Bustanji, Y.; Arciola, C. R.; Conti, M.; Mandello, E.; Montanaro, L.; Samorí, B. Dynamics of the Interaction between a Fibronectin Molecule and a Living Bacterium under Mechanical Force. *Proc. Natl. Acad. Sci. U.S.A.* **2003**, *100*, 13292–13297.
34. Yongsunthon, R.; Fowler, V. G., Jr; Lower, B. H.; Vellano, F. P., III; Alexander, E.; Reller, L. B.; Corey, G. R.; Lower, S. K. Correlation between Fundamental Binding Forces and Clinical Prognosis of *Staphylococcus aureus* Infections of Medical Implants. *Langmuir* **2007**, *23*, 2289–2292.
35. Busscher, H. J.; Van De Belt-Gritter, B.; Dijkstra, R. J. B.; Norde, W.; Petersen, F. C.; Scheie, A. A.; Van Der Mei, H. C. Intermolecular Forces and Enthalpies in the Adhesion of *Streptococcus mutans* and an Antigen I/II-Deficient Mutant to Laminin Films. *J. Bacteriol.* **2007**, *189*, 2988–2995.
36. Xu, C. P.; Van De Belt-Gritter, B.; Dijkstra, R. J. B.; Norde, W.; Van Der Mei, H. C.; Busscher, H. J. Interaction Forces between Salivary Proteins and *Streptococcus mutans* with and without Antigen I/II. *Langmuir* **2007**, *23*, 9423–9428.
37. Alsteens, D.; Dupres, V.; Klotz, S. A.; Gaur, N. K.; Lipke, P. N.; Dufrêne, Y. F. Unfolding Individual Als5p Adhesion Proteins on Live Cells. *ACS Nano* **2009**, *3*, 1677–1682.
38. Alsteens, D.; Garcia, M. C.; Lipke, P. N.; Dufrêne, Y. F. Force-Induced Formation and Propagation of Adhesion Nanodomains in Living Fungal Cells. *Proc. Natl. Acad. Sci. U.S.A.* **2010**, *107*, 20744–20749.
39. Alsteens, D.; Ramsook, C. B.; Lipke, P. N.; Dufrêne, Y. F. Unzipping a Functional Microbial Amyloid. *ACS Nano* **2012**, *6*, 7703–7711.
40. Beaussart, A.; Alsteens, D.; El-Kirat-Chatel, S.; Lipke, P. N.; Kucharíková, S.; Van Dijck, P.; Dufrêne, Y. F. Single-Molecule Imaging and Functional Analysis of Als Adhesins and Mannans During *Candida albicans* Morphogenesis. *ACS Nano* **2012**, *6*, 10950–10964.
41. Rief, M.; Gautel, M.; Oesterhelt, F.; Fernandez, J. M.; Gaub, H. E. Reversible Unfolding of Individual Titin Immunoglobulin Domains by AFM. *Science* **1997**, *276*, 1109–1112.
42. Oberhauser, A. F.; Marszalek, P. E.; Erickson, H. P.; Fernandez, J. M. The Molecular Elasticity of the Extracellular Matrix Protein Tenascin. *Nature* **1998**, *393*, 181–185.
43. Rief, M.; Pascual, J.; Saraste, M.; Gaub, H. E. Single Molecule Force Spectroscopy of Spectrin Repeats: Low Unfolding Forces in Helix Bundles. *J. Mol. Biol.* **1999**, *286*, 553–561.
44. Alegre-Cebollada, J.; Badilla, C. L.; Fernández, J. M. Isopeptide Bonds Block the Mechanical Extension of Pili in Pathogenic *Streptococcus pyogenes*. *J. Biol. Chem.* **2010**, *285*, 11235–11242.
45. Hinterdorfer, P.; Dufrêne, Y. F. Detection and Localization of Single Molecular Recognition Events Using Atomic Force Microscopy. *Nat. Methods* **2006**, *3*, 347–355.
46. Merkel, R.; Nassoy, P.; Leung, A.; Ritchie, K.; Evans, E. Energy Landscapes of Receptor-Ligand Bonds Explored with Dynamic Force Spectroscopy. *Nature* **1999**, *397*, 50–53.
47. Müller, D. J.; Helenius, J.; Alsteens, D.; Dufrêne, Y. F. Force Probing Surfaces of Living Cells to Molecular Resolution. *Nat. Chem. Biol.* **2009**, *5*, 383–390.
48. Baumgartner, W.; Hinterdorfer, P.; Ness, W.; Raab, A.; Vestweber, D.; Schindler, H.; Drenckhahn, D. Cadherin Interaction Probed by Atomic Force Microscopy. *Proc. Natl. Acad. Sci. U.S.A.* **2000**, *97*, 4005–4010.
49. Sieben, C.; Kappel, C.; Zhu, R.; Wozniak, A.; Rankl, C.; Hinterdorfer, P.; Grubmüller, H.; Herrmann, A. Influenza Virus Binds Its Host Cell Using Multiple Dynamic Interactions. *Proc. Natl. Acad. Sci. U.S.A.* **2012**, *109*, 13626–13631.
50. Telford, J. L.; Barocchi, M. A.; Margarit, I.; Rappuoli, R.; Grandi, G. Pili in Gram-Positive Pathogens. *Nat. Rev. Microbiol.* **2006**, *4*, 509–519.
51. Tripathi, P.; Dupres, V.; Beaussart, A.; Lebeer, S.; Claes, I. J. J.; Vanderleyden, J.; Dufrêne, Y. F. Deciphering the Nanometer-Scale Organization and Assembly of *Lactobacillus rhamnosus* GG Pili Using Atomic Force Microscopy. *Langmuir* **2012**, *28*, 2211–2216.
52. Steppich, D. M.; Angerer, J. I.; Sritharan, K.; Schneider, S. W.; Thalhammer, S.; Wixforth, A.; Alexander-Katz, A.; Schneider, M. F. Relaxation of Ultralarge VWF Bundles in a Microfluidic-AFM Hybrid Reactor. *Biochem. Biophys. Res. Commun.* **2008**, *369*, 507–512.

53. Craig, L.; Pique, M. E.; Tainer, J. A. Type IV Pilus Structure and Bacterial Pathogenicity. *Nat. Rev. Microbiol.* **2004**, *2*, 363–378.
54. von Ossowski, I.; Satokari, R.; Reunanen, J.; Lebeer, S.; De Keersmaecker, S. C. J.; Vanderleyden, J.; de Vos, W. M.; Palva, A. Functional Characterization of a Mucus-Specific LPXTG Surface Adhesin from Probiotic *Lactobacillus rhamnosus* GG. *Appl. Environ. Microbiol.* **2011**, *77*, 4465–4472.
55. Douillard, F. P.; Ribbera, A.; Järvinen, H. M.; Kant, R.; Pietilä, T. E.; Randazzo, C.; Paulin, L.; Laine, P. K.; Caggia, C.; von Ossowski, I.; *et al.* Comparative Genomic and Functional Analysis of *Lactobacillus casei* and *Lactobacillus rhamnosus* Strains Marketed as Probiotics. *Appl. Environ. Microbiol.* **2013**, *79*, 1923–1933.
56. Olsén, A.; Jonsson, A.; Normark, S. Fibronectin Binding Mediated by a Novel Class of Surface Organelles on *Escherichia coli*. *Nature* **1989**, *338*, 652–655.
57. Patti, J. M.; Höök, M. Microbial Adhesins Recognizing Extracellular Matrix Macromolecules. *Curr. Opin. Cell Biol.* **1994**, *6*, 752–758.
58. Bessen, D. E.; Kalia, A. Genomic Localization of a T Serotype Locus to a Recombinatorial Zone Encoding Extracellular Matrix-Binding Proteins in *Streptococcus pyogenes*. *Infect. Immun.* **2002**, *70*, 1159–1167.
59. Schwarz-Linek, U.; Werner, J. M.; Pickford, A. R.; Gurusiddappa, S.; Kim, J. H.; Pilka, E. S.; Briggs, J. A. G.; Gough, T. S.; Höök, M.; Campbell, I. D.; *et al.* Pathogenic Bacteria Attach to Human Fibronectin through a Tandem β-Zipper. *Nature* **2003**, *423*, 177–181.
60. Hilleringmann, M.; Giusti, F.; Baudner, B. C.; Masignani, V.; Covacci, A.; Rappuoli, R.; Barocchi, M. A.; Ferlenghi, I. Pneumococcal Pili Are Composed of Protofilaments Exposing Adhesive Clusters of Rrg A. *PLoS Pathog.* **2008**, *4*, e1000026.
61. Vélez, M. P.; De Keersmaecker, S. C. J.; Vanderleyden, J. Adherence Factors of *Lactobacillus* in the Human Gastrointestinal Tract. *FEMS Microbiol. Lett.* **2007**, *276*, 140–148.
62. Vélez, M. P.; Petrova, M. I.; Lebeer, S.; Verhoeven, T. L. A.; Claes, I.; Lambrichts, I.; Tynkkynen, S.; Vanderleyden, J.; De Keersmaecker, S. C. J. Characterization of MabA, a Modulator of *Lactobacillus rhamnosus* GG Adhesion and Biofilm Formation. *FEMS Immunol. Med. Microbiol.* **2010**, *59*, 386–398.
63. Kellermayer, M. S. Z.; Grama, L.; Karsai, A.; Nagy, A.; Kahn, A.; Datki, Z. L.; Penke, B. Reversible Mechanical Unzipping of Amyloid β-Fibrils. *J. Biol. Chem.* **2005**, *280*, 8464–8470.
64. Hugel, T.; Grosholz, M.; Clausen-Schaumann, H.; Pfau, A.; Gaub, H.; Seitz, M. Elasticity of Single Polyelectrolyte Chains and Their Desorption from Solid Supports Studied by AFM Based Single Molecule Force Spectroscopy. *Macromolecules* **2001**, *34*, 1039–1047.
65. Rief, M.; Clausen-Schaumann, H.; Gaub, H. E. Sequence-Dependent Mechanics of Single DNA Molecules. *Nat. Struct. Biol.* **1999**, *6*, 346–349.
66. Proft, T.; Baker, E. N. Pili in Gram-Negative and Gram-Positive Bacteria: Structure, Assembly and Their Role in Disease. *Cell. Mol. Life Sci.* **2009**, *66*, 613–635.
67. Merz, A. J.; So, M.; Sheetz, M. P. Pilus Retraction Powers Bacterial Twitching Motility. *Nature* **2000**, *407*, 98–102.
68. Biais, N.; Ladoux, B.; Higashi, D.; So, M.; Sheetz, M. Cooperative Retraction of Bundled Type IV Pili Enables Nanonewton Force Generation. *PLoS Biol.* **2008**, *6*, 907–913.
69. Dufrêne, Y. F. Atomic Force Microscopy and Chemical Force Microscopy of Microbial Cells. *Nat. Protoc.* **2008**, *3*, 1132–1138.
70. Ebner, A.; Wildling, L.; Kamruzzahan, A. S. M.; Rankl, C.; Wruss, J.; Hahn, C. D.; Hölzl, M.; Zhu, R.; Kienberger, F.; Blaas, D.; *et al.* A New, Simple Method for Linking of Antibodies to Atomic Force Microscopy Tips. *Bioconjugate Chem.* **2007**, *18*, 1176–1184.